

## Article

# Room-Temperature Eutectic Synthesis for Upcycling of Cathode Materials

W. Blake Hawley <sup>1,2</sup>, Mengya Li <sup>1</sup>  and Jianlin Li <sup>1,\*</sup> 

<sup>1</sup> Oak Ridge National Laboratory, Electrification and Energy Infrastructures Division, Oak Ridge, TN 37831, USA; hawleywb@ornl.gov (W.B.H.); lim1@ornl.gov (M.L.)

<sup>2</sup> Bredesen Center for Interdisciplinary Research and Graduate Education, University of Tennessee, Knoxville, TN 37996, USA

\* Correspondence: lij4@ornl.gov

**Abstract:** Ni-rich  $\text{LiNi}_x\text{Mn}_y\text{Co}_{1-x-y}\text{O}_2$  (NMC) materials have been adopted in a range of applications, including electric vehicles. The recycled NMC material from a spent cell would be much more valuable if it could be upgraded to a Ni-rich, more energy-dense version of the material. This work demonstrates a simple, inexpensive, and facile method to upcycle  $\text{LiNi}_{1/3}\text{Mn}_{1/3}\text{Co}_{1/3}\text{O}_2$  (NMC111, 160  $\text{mAh}\cdot\text{g}^{-1}$ ), a cathode used in early generations of electric vehicle batteries, to  $\text{LiNi}_{0.8}\text{Mn}_{0.1}\text{Co}_{0.1}\text{O}_2$  (NMC811, 190  $\text{mAh}\cdot\text{g}^{-1}$ ), a more energy-dense cathode material. In this study, a preliminary investigation into a room-temperature eutectic synthesis of NMC811 is performed using NMC111, LiOH, and nickel nitrate as precursors. The synthesized material showed the desired crystal structure and stoichiometry, though the cycle life and Li diffusion coefficient need improvement when compared to commercially available NMC811. This study demonstrates an interesting proof of concept of the room-temperature eutectic synthesis process for LIB cathodes and could be improved by tuning the synthesis conditions.

**Keywords:** eutectic synthesis; room-temperature synthesis; Ni-rich cathode; battery recycling; lithium-ion battery



**Citation:** Hawley, W.B.; Li, M.; Li, J. Room-Temperature Eutectic Synthesis for Upcycling of Cathode Materials. *Batteries* **2023**, *9*, 498. <https://doi.org/10.3390/batteries9100498>

Academic Editor: Qing Wang

Received: 23 August 2023

Revised: 18 September 2023

Accepted: 25 September 2023

Published: 28 September 2023



**Copyright:** © 2023 by the authors. Licensee MDPI, Basel, Switzerland. This article is an open access article distributed under the terms and conditions of the Creative Commons Attribution (CC BY) license (<https://creativecommons.org/licenses/by/4.0/>).

## 1. Introduction

The ever-expanding lithium-ion battery (LIB) market requires a growth in LIB production capacity, which not only consumes critical expensive metals but also generates an enormous number of end-of-life LIBs. Thus, there is growing interest and effort in developing new electrode materials with low Co content [1] or organic cathode materials [2,3], and recycling materials from spent batteries [4–6]. Particular efforts have been made to recycle valuable elements [7–9] and compounds [10–13], respectively. Meanwhile, the continuous demand for longer driving ranges has motivated material development [14] and cell engineering to increase energy density [15,16]. For instance, low Ni content  $\text{LiNi}_x\text{Mn}_y\text{Co}_{1-x-y}\text{O}_2$  (NMC) (e.g., NMC111 and NMC532) was a typical material used in early generation electric vehicle batteries [17]. However, high Ni content NMC ( $x \geq 0.6$ ) is the state-of-the-art cathode material for high energy density applications and has been adopted in recent electric vehicle batteries [18]. Compared to NMC111, NMC811 poses a higher attainable specific capacity of 190  $\text{mAh}\cdot\text{g}^{-1}$  (at room temperature and C/10 discharge rate for industrially-relevant active mass loadings) and higher energy density [19]. When the original generation of electric vehicle batteries using low Ni content NMC materials reach their end-of-life (EOL), it would be advantageous to not only recycle these cathode materials but also “upcycle” the lower-capacity formulation into the state-of-art materials, like NMC811.

Lower-capacity cathode formulations, like NMC111, can be upgraded through either resynthesis using salts recovered from a hydrometallurgical process or a direct upcycling

method. The former process requires the use of corrosive acid and energy-intensive calcination steps, leaving a larger carbon footprint. Various methods have been reported in upcycling cathode materials including solid-state sintering [20], hydrothermal, and deep eutectic solvents [21]. Solid-state sintering is easy to operate but has challenges in homogeneity and slow ion diffusion in the solid phase. Thus, it requires a higher temperature and longer sintering time. The hydrothermal method can mix the precursors homogeneously but may require multiple steps in rinsing and sintering under high pressure (i.e., in autoclaves). Deep eutectic solvents are formed from a eutectic mixture of Lewis or Bronsted acids and bases, which has a low melting point owing to the charge delocalization through hydrogen bonding [22]. This can improve the homogeneity of the synthesized product and reduce the sintering temperature. However, some solvents could be expensive [6]. Dai et al. developed a “reciprocal ternary molten salts” system to directly upcycle spent NMC111 to NMC622 by simultaneously realizing the addition of Ni and the relithiation of Li in spent NMC111 [21]. However, this process utilized molten salts as flux media, which potentially increased the processing cost. Therefore, it is important to develop a simple yet effective, and energy-efficient process to upgrade the cathode chemistries.

In this study, we propose to upcycle NMC111 to NMC811 via eutectic synthesis, which can form a eutectic solution at room temperature and reduce energy consumption in the upcycling process. Meanwhile, the eutectic solution renders good mixing of the precursors and NMC111 to improve composition homogeneity. The eutectic method has been used in synthesizing materials. Fang et al. used eutectic synthesis to fabricate  $\text{LiNi}_{0.5}\text{Mn}_{1.5}\text{O}_4$  (LNMO) cathode material from  $\text{Ni}(\text{CH}_3\text{CO}_2)_2 \cdot 4\text{H}_2\text{O}$ ,  $\text{Mn}(\text{CH}_3\text{CO}_2)_2 \cdot 4\text{H}_2\text{O}$ , and  $\text{Li}(\text{CH}_3\text{CO}_2) \cdot 2\text{H}_2\text{O}$ . They discovered that these three materials form a eutectic alloy at 80 °C, as seen by the formation of a green slurry. At low sintering temperatures (700 °C), nano-sized LNMO capable of high rate capability was formed; conversely, at high sintering temperatures (900 °C), micron-sized LNMO with stable cycle life performance was created [23]. More recently, Li et al. used eutectic synthesis to fabricate the P2-type  $\text{Na}_x\text{Fe}_{1/2}\text{Mn}_{1/2}\text{O}_2$  cathode for sodium-ion batteries. In their study,  $\text{NaOH}$ ,  $\text{Fe}(\text{NO}_3)_3 \cdot 9\text{H}_2\text{O}$ , and  $\text{Mn}(\text{NO}_3)_2 \cdot 4\text{H}_2\text{O}$  were combined in a mortar and formed a eutectic at room temperature. Two calcination steps were necessary: the first was used to remove the nitrates from the material and the second was to form the pure phase. The material they synthesized possessed a higher  $\text{Na}^+$  diffusivity and lower charge transfer resistance at the electrolyte/Na metal interface and cathode/electrolyte interface than its sol-gel synthesized baseline [24].

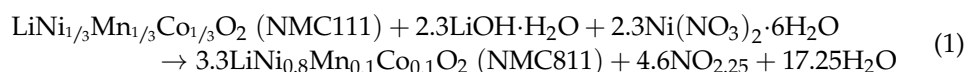
In this study, NMC811 was synthesized using eutectic synthesis from NMC111,  $\text{LiOH}$ , and nickel nitrate as precursors. Pristine NMC111 was used as a precursor since EOL NMC111 was unavailable for this study. However, the demonstrated upcycling method should be applicable for spent NMC111 with minor modifications on precursor compositions. Thus, the findings are still meaningful for the upcycling of spent cathodes. Additionally, while this study was designed with battery recycling in mind, the process also has applications in upcycling battery scraps during the manufacturing of either cathode active materials or electrodes. This synthesis method enables faster, less expensive upcycling of Ni-deficient materials than the more traditional synthesis techniques. The characterization of the material proves that the desired crystal structure and stoichiometry are achieved. The electrochemical performance of the material, however, is still poorer than commercially-available NMC811. Further tuning of the synthesis conditions and finer control over the particle size could help resolve this performance deficiency in future iterations of the technique.

## 2. Experimental Section

### 2.1. Eutectic Synthesis

The materials used in the eutectic synthesis were  $\text{LiOH} \cdot \text{H}_2\text{O}$  (Sigma Aldrich, St. Louis, MO, USA),  $\text{Ni}(\text{NO}_3)_2 \cdot 6\text{H}_2\text{O}$  (Sigma Aldrich), and NMC111 (Targray,  $d_{50} = 6.5 \mu\text{m}$ ). In the first step, appropriate amounts of  $\text{LiOH} \cdot \text{H}_2\text{O}$  and  $\text{Ni}(\text{NO}_3)_2 \cdot 6\text{H}_2\text{O}$  were added to a mortar and combined using a pestle. After several minutes of muddling, the mixture

became a low-viscosity green slurry. Next, NMC111 was added and mixed further with the pestle. Initially, the mixture was a low-viscosity black slurry, but after a few minutes of stirring, became a more viscous slurry. This slurry was calcined at 400 °C for 6 h (2.5 °C·min<sup>-1</sup>) in ambient air to remove the nitrates from the slurry. Once finished, the product became gravel-like particles that were muddled with the mortar and pestle. These muddled powders were sintered again at 850 °C for 12 h (2.5 °C·min<sup>-1</sup>) in flowing O<sub>2</sub> (1.0 SLM). The total reaction is written in Equation (1).



A 10 mol% excess of LiOH·H<sub>2</sub>O was used in order to overcome the well-documented issue of cation mixing (Ni<sup>2+</sup>/Li<sup>+</sup>) in the structure of Ni-rich materials [25]. The material synthesized via eutectic synthesis will henceforth be referred to as ES-NMC811. Once the second sintering step was completed, the powders were mixed again with the mortar and pestle. The powders were then sieved through a 50 µm mesh to ensure an appropriate particle size.

## 2.2. Material Characterization

The crystal structure of the ES-NMC811 was examined using an X-ray diffractometer (XRD, PANalytical X'PERT, Malvern Panalytical Inc., Westborough, MA, USA) operating at 45 kV and 40 mA and utilizing a Cu source ( $\lambda = 1.54 \text{ \AA}$ ). Diffraction patterns were recorded between  $2\theta$  of 10° and 60° at room temperature with a 0.016° step size. The elemental composition of the powders was determined using inductively coupled plasma-optical emission spectroscopy (ICP-OES, Agilent Technologies 5110, Santa Clara, CA, USA). The samples were digested in an aqua regia solution and then diluted in 2 wt% HNO<sub>3</sub> for ICP measurement. The particle morphology was analyzed using a Zeiss-MERLIN™ field-emission scanning electron microscope (SEM, ZEISS Microscopy, Pleasanton, CA, USA). The structure of the particle surfaces was examined using a transmission electron microscope (TEM).

## 2.3. Electrochemical Characterization

Composite cathodes were made by mixing ES-NMC811 with N-methyl-pyrrolidone (Sigma Aldrich) as the solvent, carbon black (CB, Denka Li-100) as a conductive additive, and polyvinylidene fluoride (PVDF, APV Engineered Coatings, 8.0 wt% pre-dispersed in NMP) as the binder. The cathode slurries were made with 45 wt% solids content, of which 90 wt% was active material, 5 wt% was CB, and 5 wt% was PVDF, and were mixed in a high-energy ball mill (SPEX Sample Prep 8000M Mixer/Mill) for 30 min total. The cathode slurries were coated onto Al foil (15 µm thick, MTI Corp., Richmond, CA, USA) using a film applicator (Qualtech Products Industry, Denver, CO, USA) with a 200 µm wet gap. The coatings were dried overnight in a fume hood followed by 2 h in a vacuum oven at 100 °C. After drying, the active mass loading of the cathodes was approximately 6.3 mg·cm<sup>-2</sup>. This led to an areal capacity of the cathodes of roughly 1.2 mAh·cm<sup>-2</sup>, assuming a specific capacity of 190 mAh·g<sup>-1</sup> for ES-NMC811. To compare with the ES-NMC811 material, a composite cathode with commercially available NMC811 (Targray, d<sub>50</sub> = 13.8 µm) was made according to the same cathode recipe. Additionally, cells were constructed with the commercially available NMC111 for comparison with the precursor material. The commercially available NMC materials will henceforth be denoted as “CA-NMC”. All subsequent electrochemical testing was performed in an ESPEC battery testing chamber at 30 °C.

Using the same materials above, half coin cells were built; three drops of electrolyte were added to each side of the separator. Three cells of each material were subject to a cycle life protocol. Three formation cycles were performed between 3.0 and 4.3 V at +0.1 C/−0.1 C; these formation cycles were followed by 50 cycles at +0.5 C/−0.5 C between the same potential limits. After constant-current (CC) charging to 4.3 V, the cells were charged in a constant-

voltage (CV) step for an additional 30 min or until the current dropped below C/20. After charge and discharge, cells rested for 15 min. Three cells of each material were cycled to ensure statistically significant results. For all tests utilizing multiple cells, the standard deviation of the capacity at a particular cycle number is used as the error bar.

In addition to the cycling tests, three coin cells were built for galvanostatic intermittent titration technique (GITT) analysis. GITT consists of two steps: (1) A step charging the cell for 1 h to a specific state of charge (SOC), and (2) A step of relaxation for 2 h. These steps were repeated until the cell reached the upper cutoff potential, then were repeated as the cell was discharged to the lower cutoff potential, with the cell being discharged to a particular depth of discharge (DOD) at each step.

### 3. Results and Discussion

#### 3.1. Material Properties

To determine if the synthesized material was structurally and stoichiometrically NMC811, a suite of material characterizations was performed. First, the stoichiometry of the ES-NMC811 sample was measured using ICP-OES. The exact formula of the ES-NMC811 was  $\text{Li}_{0.983}\text{Ni}_{0.779}\text{Mn}_{0.111}\text{Co}_{0.110}\text{O}_2$ , which is very similar to NMC811. It is worth mentioning that the ICP-OES is an average result. While it confirms the average composition, it does not provide information on composition homogeneity. In reality, spent cathode materials are likely not homogeneous in compositions and are more challenging to synthesize into uniform products compared to those with uniform starting compositions.

The diffraction patterns for the ES-NMC811, CA-NMC111, and CA-NMC811, are shown in Figure 1. All three materials exhibited a layered oxide crystal structure with hexagonal  $\alpha\text{-NaFeO}_2$  structure and space group  $R\bar{3}m$ . An important feature of the diffractograms is the intensity ratio between the (003) peak ( $I_{003}$ ) and the (104) peak ( $I_{104}$ ). The  $I_{003}/I_{104}$  ratio is indicative of the degree of cation mixing in the active material; an  $I_{003}/I_{104} > 1.2$  suggests a low degree of cation mixing in the material [26]. The intensity ratios for the CA-NMC811 and ES-NMC811 are 1.70 and 1.58, respectively, indicating excellent order in the structure. Additionally, the (006) and (102) peaks should be well-resolved in a material with good order in the crystal structure, which is also observed in both structures.

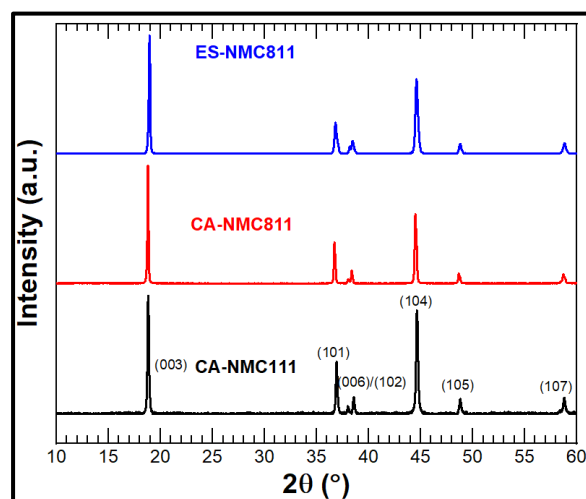


**Figure 1.** XRD patterns of the CA-NMC111, CA-NMC811, and ES-NMC811.

Good Li-ion transport in NMC materials is highly dependent on the level of cation mixing. Cation mixing between  $\text{Li}^+$  and  $\text{Ni}^{2+}$  ions, which have similar ionic radii (76 pm and 69 pm with coordination number = 6, respectively [27]), results in reducing the Li layer spacing which harms Li diffusion. The differences in crystal structure could arise from residence time in the tube furnace after cooling, the existence of “hot spots” in the tube furnace, or differences in the amount of and/or purity of  $\text{O}_2$  in the environment.

The materials were imaged using SEM (see Figure 2) and TEM (see Figure 3). The CA-NMC111 secondary particles are roughly spherical, though the primary particles are somewhat indistinguishable (see Figure 2a,b). In the ES-NMC811 samples, the secondary particles are more of a polyhedral shape, though the primary particles are roughly spherical (see Figure 2c,d). The long muddling times in the mortar and pestle likely distorted the secondary ES-NMC811 particles from their spherical shape. Since particle morphology plays an important role in material performance [28–30], granulation may be required to achieve desirable particle morphology, size, and shape. Though not measured, the particle size distribution in the ES-NMC811 particles varied significantly according to the collected images, while the CA powders were generally within a tighter distribution. This is likely a product of the sophistication of the processes and equipment used in industrial cathode material production. Beyond this proof-of-concept study, future work will investigate the effect of the heating and cooling rate and the temperature in the calcination steps on the particle size.

The TEM images reveal good ordering at the surface of both the CA-NMC811 and ES-NMC811 material (see Figure 3). This correlates well with the ICP-OES, XRD, and SEM data. However, the layer spacing between the two materials seems to be different. The average layer spacing in the ES-NMC811 material is approximately  $3.0\text{ \AA}$ , while the average layer spacing in the CA-NMC811 material is shorter at  $2.5\text{ \AA}$ . The slight difference in layer spacing could be a cause for the subpar electrochemical performance in the ES-NMC811 material, as discussed in the following section. Still, the material properties of the ES-NMC811 are quite similar to the CA-NMC811 material. With proper optimization of the conditions, eutectic synthesis could be a time and energy-efficient means of upcycling spent cathode materials.

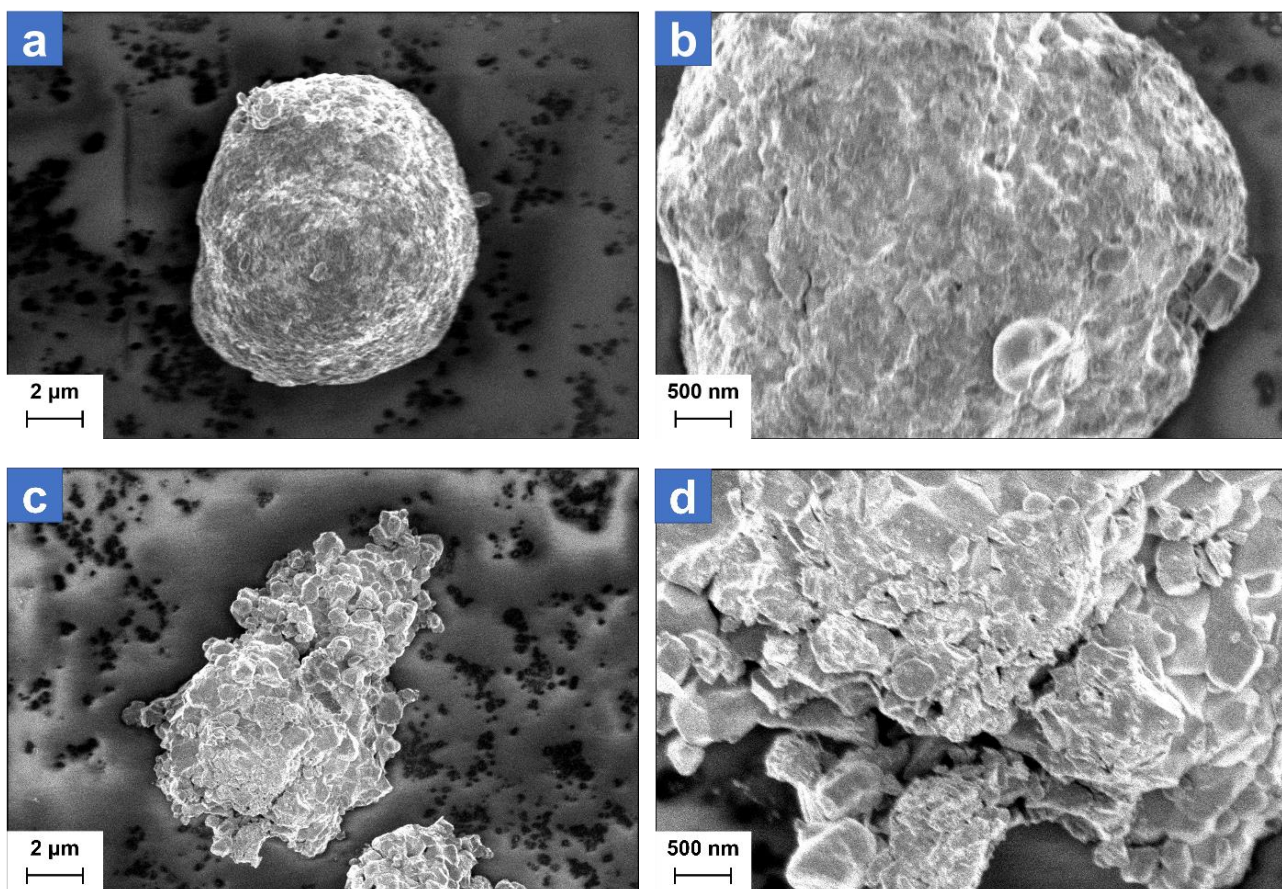


**Figure 2.** SEM images of (a,b) CA-NMC111 and (c,d) ES-NMC811.

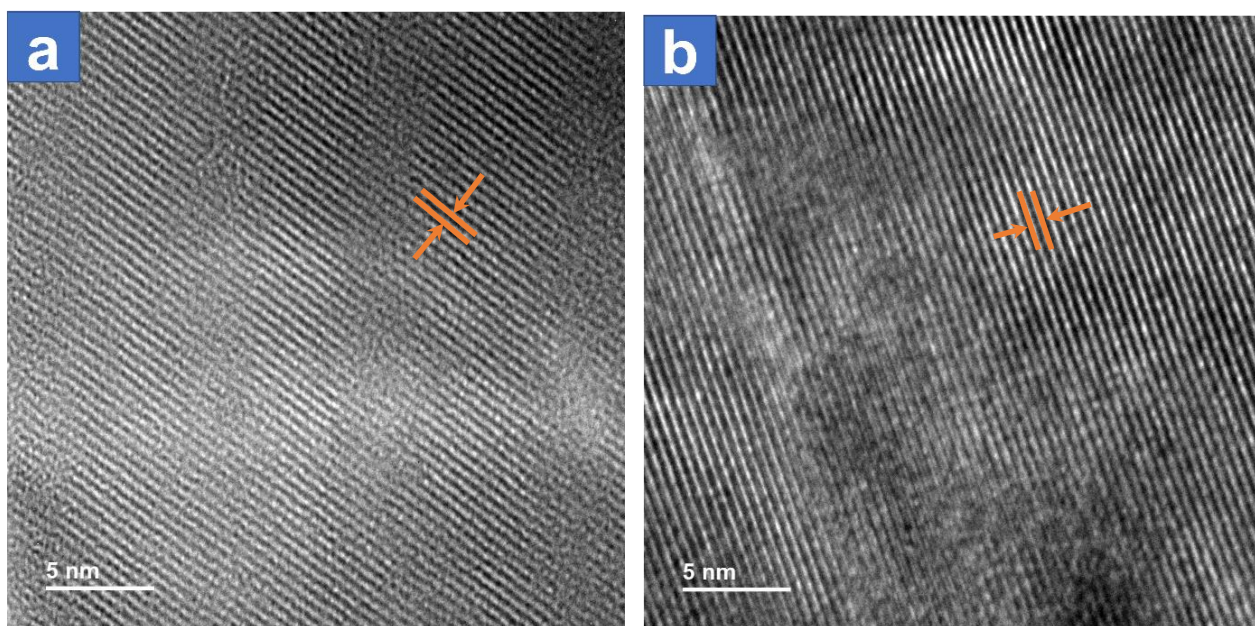


**Figure 3.** TEM images of (a) CA-NMC811 and (b) ES-NMC811. The layer spacing in the CA-NMC811 ( $2.5\text{ \AA}$ ) is slightly shorter than that in the ES-NMC811 ( $3.0\text{ \AA}$ ) and is indicated by the red arrows in the images.

### 3.2. Electrochemical Properties

The cycle life of the ES-NMC811 was evaluated (see Figure 4a–c). During the three formation cycles, ( $+0.1\text{ C}/-0.1\text{ C}$ , approximately  $+0.185\text{ mA}/-0.185\text{ mA}$ ), the discharge capacity was  $172.7$ ,  $171.7$ , and  $170.6\text{ mAh}\cdot\text{g}^{-1}$ , respectively. One would expect a discharge capacity of  $\geq 190\text{ mAh}\cdot\text{g}^{-1}$  at such a low current density for NMC811 [19]. During cycling ( $+0.5\text{ C}/-0.5\text{ C}$ , approximately  $+0.923\text{ mA}/-0.923\text{ mA}$ ), the initial discharge capacity was  $158.2\text{ mAh}\cdot\text{g}^{-1}$  and dropped to below 80% of its initial capacity at only the 35th cycle (see Figure 4a). The point at which a cell reaches 80% of its initial capacity is commonly used to indicate a cell's EOL condition. Therefore, for the cells to only last 35 cycles before reaching EOL indicates the need for significant improvement.

Comparing these data with the cycling performance of the precursor CA-NMC111 material, the capacity during the formation cycles was  $158.5$ ,  $159.0$ , and  $158.9\text{ mAh}\cdot\text{g}^{-1}$ , respectively. As expected, the more Ni-rich ES-NMC811 material achieves significantly higher discharge capacity, since the  $\text{Ni}^{2+}/\text{Ni}^{4+}$  redox reactions provide the most capacity within the selected potential window. During cycling, the initial capacity of the CA-NMC111 material was  $147.4\text{ mAh}\cdot\text{g}^{-1}$  but faded to only  $145.5\text{ mAh}\cdot\text{g}^{-1}$  (98.7% retention) by the 35th cycle. Since the Ni-rich materials undergo additional phase transformations at higher potentials, causing irreversible structural rearrangement [31], it is unsurprising that the more Ni-deficient material would have a longer cell lifetime than the more Ni-rich material. Therefore, a comparison with CA-NMC811 is appropriate. During the three formation cycles, this cell achieved a capacity of  $196.3$ ,  $198.7$ , and  $195.4\text{ mAh}\cdot\text{g}^{-1}$ , which is about a 14% improvement over ES-NMC811. After 35 cycles, the CA-NMC811 cell delivered  $179.1\text{ mAh}\cdot\text{g}^{-1}$ , which was 95.8% of its first-cycle capacity. This is a decrease in capacity retention from CA-NMC111 but is still substantially better than ES-NMC811. These results suggest that the cyclability of ES-NMC811 must be improved and that the capacity is low for a material with its chemistry.

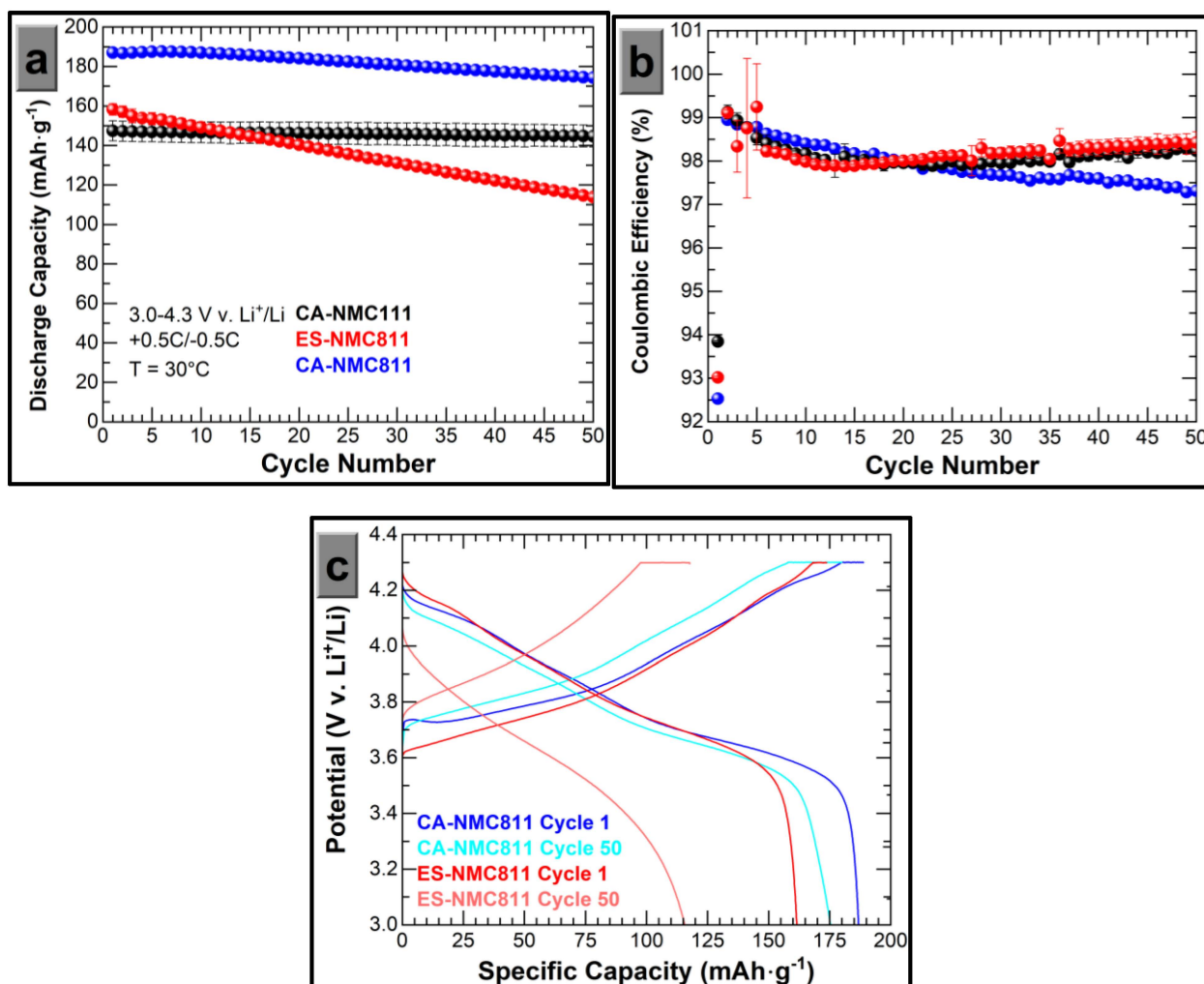


**Figure 4.** (a) Discharge capacity and (b) Coulombic efficiency of the 50 cycles of the half cells made with CA-NMC111 (black), ES-NMC811 (red), and CA-NMC811 (blue) cathodes. (c) Charge/discharge curves for the 1st and 50th cycle of the CA-NMC811 (blue and cyan, respectively) and best-performing ES-NMC811 half cell (red and light red, respectively).

The Coulombic efficiency of CA-NMC111, ES-NMC811, and CA-NMC811 is relatively low (<99%) in nearly all 50 cycles due to the reactivity of the Li counter electrode (see Figure 4b) [32]. All cells have a relatively low first-cycle Coulombic efficiency, which is typical for the first cycle after formation when the current density is increased. Interestingly, the CA-NMC111 and ES-NMC811 follow similar trends in Coulombic efficiency. For cycles 2–10, the efficiency decreases to a value of 97.5%, then increases steadily to 98.5% by the 50th cycle. Conversely, the Coulombic efficiency of the CA-NMC811 material decreases from its maximum value in the second cycle (~99%) to a minimum of 97.3% in the 50th cycle. The Coulombic efficiency is a measure of the side reactions in the cell, some of which involve the cathode active material and the electrolyte. Since the ES-NMC811 particles have a different size and morphology compared to the CA-NMC811 particles, the surface chemistry occurring between the active material and the electrolyte is likely to be different. As mentioned previously, NMC811 becomes unstable at high upper cutoff voltage due to the presence of Ni<sup>4+</sup> at the surface of the particle, which explains the discrepancy in Coulombic efficiency between CA-NMC111 and CA-NMC811.

The potential vs. specific capacity curves for the first and 50th cycles of a representative half-cell from the group of CA-NMC811 and ES-NMC811 cells show a stark contrast in the progression of the cell resistance (see Figure 4c). The initial cell potential in the

charge and discharge steps increases by nearly 150 mV and decreases by nearly 200 mV, respectively, between the first and 50th cycles for the ES-NMC811 cell. Conversely, there is little difference in the initial charge and discharge potentials for the CA-NMC811 cell. Considering the cells are cycled at the same C-rates and the cells are produced with the same components, this indicates a rapid rise in resistance that is contributed by the ES-NMC811 cathode material. Additionally, the absolute values of the slopes of the 50th charge/discharge curves are much higher than those of the first charge/discharge curves for the ES-NMC811 cell. This means that less capacity is being extracted from each redox reaction. When coupled with the aforementioned voltage fade between the first and 50th cycles, the reversibility of the reactions in the cathode active material is impaired significantly for ES-NMC811. The final feature of note is the ratio of the CV charge capacity to the CC charge capacity. The ratio increases from 3.4% in the 1st cycle to 18.6% in the 50th cycle for the ES-NMC811 cell, whereas the ratio increases from 4.8% to 12.2% in the CA-NMC811 cell. More capacity being extracted from the CV step further signals the relatively greater rise in internal resistance for the ES-NMC811 cell compared to the CA-NMC811 cell.

For the half-cells, a GITT protocol was enacted after formation to determine the Li<sup>+</sup> diffusion coefficient ( $D$ ), which is defined as the square of the average diffusion length ( $L$ ) divided by the time required for diffusion ( $t$ ) (see Equation (2)).

$$D = \frac{L^2}{t} \quad (2)$$

Assuming spherical particles, the diffusion length is the average particle radius. The radius of 20 particles was measured using SEM and was determined to be 3.46 μm; this estimate was used as the average diffusion length. After the 1 h charge in the GITT protocol, the potential decays rapidly before reaching a steady state; similarly, during the discharge steps, after the 1 h discharge, the potential increases rapidly before reaching a steady state. The initial potential ( $E_0$ ) and steady-state potential ( $E_\infty$ ) can be related to the diffusion time according to Equation (3).

$$\ln(E_0 - E_\infty) = \ln(A) + \frac{8t}{\pi^2 \tau} \quad (3)$$

By plotting the potential as a function of time during the rest period and removing the initial decay and steady-state data, a region where potential varies linearly with time can be identified. The slope of the equation fitting these data can be plugged into Equation (2) and be used to calculate the diffusion coefficient according to Equation (4). The linear region of the potential vs. time plots is displayed in Figure S1 for the charge step and in Figure S2 for the discharge step.

$$D = \frac{L^2 \pi^2 \text{slope}}{8} \quad (4)$$

Tables summarizing the SOC/DOD, slope, diffusion coefficient, and potential of each rest step for the charge in discharge are displayed in Tables S1 and S2, respectively. The diffusion coefficient as a function of potential for the first charge and discharge after formation is shown in Figure 5. Between 3.6 and 4.2 V vs. Li<sup>+</sup>/Li, the diffusion coefficient for ES-NMC811 is between 1 and  $2 \times 10^{-13}$  cm<sup>2</sup>·s<sup>-1</sup>. In contrast, the charge diffusion coefficient for CA-NMC111 was found to range between 6 and  $20 \times 10^{-13}$  cm<sup>2</sup>·s<sup>-1</sup> and the discharge diffusion coefficient was found to range between 6 and  $11 \times 10^{-13}$  cm<sup>2</sup>·s<sup>-1</sup> (see Figure S3). Similarly, the charge diffusion coefficient for CA-NMC811 was found to range between 8 and  $24 \times 10^{-13}$  cm<sup>2</sup>·s<sup>-1</sup> and the discharge diffusion coefficient was found to range between 10 and  $16 \times 10^{-13}$  cm<sup>2</sup>·s<sup>-1</sup> (see Figure S4). The low diffusion coefficient of ES-NMC811 relative to the commercially available powders could be partially responsible for the poor cycle life and relatively low capacity of the material at 0.1 C and 0.5 C current densities and demonstrates an opportunity for improvement and optimization of the eutectic synthesis process.

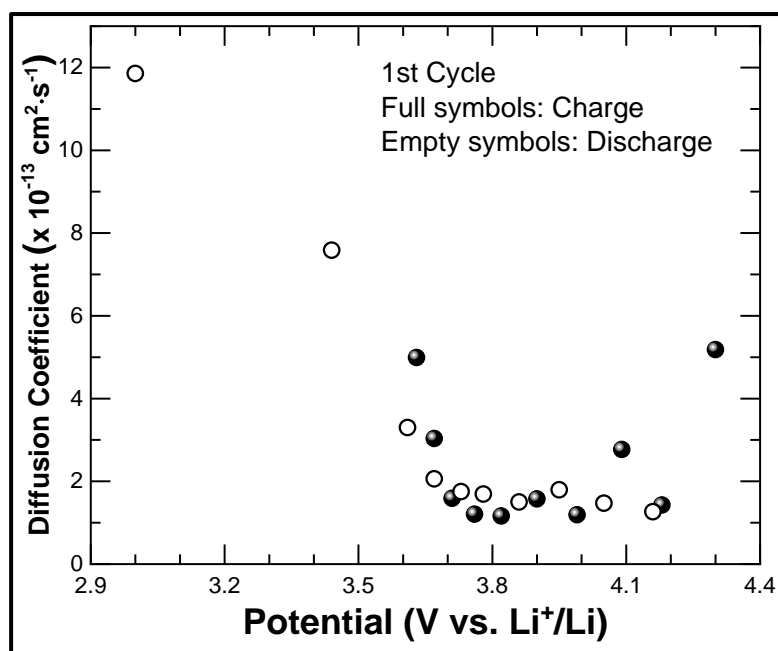


**Figure 5.** GITT data of ES-NMC811.

### 3.3. Discussion

It is worth mentioning that this work only demonstrates a proof-of-concept in upcycling cathode materials via eutectic synthesis. Compared to other methods such as solid-state sintering, hydrothermal, and deep eutectic solvents, the eutectic method can use common and low-cost precursors and form a eutectic mixture at low temperatures. This allows for low-temperature annealing. The method promises to also generate high purity and homogeneous material, which is very scalable.

However, this work only shows an extremely simplified situation where pristine NMC111 was used instead of spent NMC111. In application, the spent NMC111 could introduce many challenges including the heterogeneity in chemical composition, particle and morphology breakdown, wide particle size distribution, and contamination with impurities from the recycling process. All these could affect the material performance and need to be restored [33,34]. Much more work is required to further validate the viability of the method for practical application. Nevertheless, this work provides another compelling option for material upcycling.

### 4. Conclusions

In this study, a room-temperature eutectic synthesis method was used to upgrade NMC111 to the more Ni-rich NMC811 material. The synthesized material had minimal cation mixing and the preferred stoichiometry. The cycle life of the ES-NMC811 material was worse than that of both the precursor NMC111 material and the CA-NMC811. Additionally, the Li diffusion coefficient was lower in the ES-NMC811 material. This could be caused by unoptimized particle size and distribution or the synthesis conditions being unoptimized. This study provides a proof-of-concept that the room-temperature eutectic synthesis was shown to be capable of upcycling the NMC111 material; future investigations should investigate different synthesis conditions on the material and seek to enhance the material's structure so that its electrochemical performance may be maximized. It is possible that this same method could be used to convert from any stoichiometry of NMC material to another by adding Co or Mn-containing nitrates to the slurry. However, the most relevant case of synthesized NMC811 from NMC111 was considered, as most lithium-ion battery applications demand low-Co, energy-dense cathode active materials.

**Supplementary Materials:** The following supporting information can be downloaded at: <https://www.mdpi.com/article/10.3390/batteries9100498/s1>. Figure S1: The potential vs. time plots for the ten rest periods, executed at: (a) 10% SOC, (b) 20% SOC, (c) 30% SOC, (d) 40% SOC, (e) 50% SOC, (f) 60% SOC, (g) 70% SOC, (h) 80% SOC, (i) 90% SOC, and (j) 100% SOC. The time represents the total time of the charge/discharge cycle. The dashed black line represents the linear fit of the raw data shown with the red data points.; Figure S2: The potential vs. time plots for the ten rest periods, executed at: (a) 10% DOD, (b) 20% DOD, (c) 30% DOD, (d) 40% DOD, (e) 50% DOD, (f) 60% DOD, (g) 70% DOD, (h) 80% DOD, (i) 90% DOD, and (j) 100% DOD. The time represents the total time of the charge/discharge cycle. The dashed black line represents the linear fit of the raw data shown with the red data points. Figure S3: The diffusion coefficient determined via GITT analysis for the CA-NMC111 material. Figure S4: The diffusion coefficient determined via GITT analysis for the CA-NMC811 material. Table S1: A summary of the data from the charge step of the GITT protocol. Table S2: A summary of the data from the discharge step of the GITT protocol.

**Author Contributions:** Conceptualization, W.B.H., M.L. and J.L.; methodology, W.B.H., M.L. and J.L.; validation, W.B.H. and J.L.; formal analysis, W.B.H., M.L. and J.L.; investigation, W.B.H. and M.L.; resources, J.L.; data curation, W.B.H. and M.L.; writing-original draft preparation, W.B.H.; writing-review and editing, W.B.H., M.L. and J.L.; visualization, W.B.H., M.L. and J.L.; supervision, M.L. and J.L.; project administration, J.L.; funding acquisition, J.L. All authors have read and agreed to the published version of the manuscript.

**Funding:** This research at Oak Ridge National Laboratory (ORNL), managed by UT Battelle, LLC, for the U.S. Department of Energy under contract DE-AC05-00OR22725, was sponsored by the Office of Energy Efficiency and Renewable Energy (EERE) Vehicle Technologies Office (VTO).

**Institutional Review Board Statement:** Not applicable.

**Data Availability Statement:** The data presented in this study are available on request from the corresponding author.

**Acknowledgments:** This research at Oak Ridge National Laboratory (ORNL), managed by UT Battelle, LLC, for the U.S. Department of Energy (DOE) under contract DE-AC05-00OR22725, was sponsored by the Office of Energy Efficiency and Renewable Energy (EERE) Vehicle Technologies Office (VTO) (Applied Battery Research (ABR) Program Manager: Peter Faguy). Part of this work was conducted at the Center for Nanophase Materials Sciences (CNMS), which is sponsored at Oak Ridge National Laboratory by the Division of Scientific User Facilities, U.S. Department of Energy, managed by UT-Battelle, LLC, for the U.S. The US government retains and the publisher, by accepting the article for publication, acknowledges that the US government retains a nonexclusive, paid-up, irrevocable, worldwide license to publish or reproduce the published form of this manuscript or allow others to do so, for US government purposes. DOE will provide public access to these results of federally sponsored research in accordance with the DOE Public Access Plan (<http://energy.gov/downloads/doe-public-access-plan> (accessed on 22 August 2023)).

**Conflicts of Interest:** The authors declare no conflict of interest.

## References

1. Muralidharan, N.; Self, E.C.; Dixit, M.; Du, Z.; Essehli, R.; Amin, R.; Nanda, J.; Belharouak, I. Next-generation cobalt-free cathodes—A prospective solution to the battery industry’s cobalt problem. In *Transition Metal Oxides for Electrochemical Energy Storage*; Wiley: Hoboken, NJ, USA, 2022; pp. 33–53. [[CrossRef](#)]
2. Lyu, H.; Sun, X.-G.; Dai, S. Organic cathode materials for lithium-ion batteries: Past, present, and future. *Adv. Energy Sustain. Res.* **2021**, *2*, 2000044. [[CrossRef](#)]
3. Li, J.; Sun, X.-G. Polypeptide-based batteries toward sustainable and cyclic manufacturing. *Chem.* **2021**, *7*, 1705–1707. [[CrossRef](#)]
4. Harper, G.; Sommerville, R.; Kendrick, E.; Driscoll, L.; Slater, P.; Stolkin, R.; Walton, A.; Christensen, P.; Heidrich, O.; Lambert, S.; et al. Recycling lithium-ion batteries from electric vehicles. *Nature* **2019**, *575*, 75–86. [[CrossRef](#)]
5. Li, J.; Lu, Y.; Yang, T.; Ge, D.; Wood III, D.L.; Li, Z. Water-based electrode manufacturing and direct recycling of lithium-ion battery electrodes—A green and sustainable manufacturing system. *iScience* **2020**, *23*, 101081. [[CrossRef](#)]
6. Wang, T.; Luo, H.; Bai, Y.; Li, J.; Belharouak, I.; Dai, S. Direct recycling of spent NCM cathodes through ionothermal lithiation. *Adv. Energy Mater.* **2020**, *10*, 2001204. [[CrossRef](#)]
7. Li, L.; Zhang, X.; Li, M.; Chen, R.; Wu, F.; Amine, K.; Lu, J. The recycling of spent lithium-ion batteries: A review of current processes and technologies. *Electrochim. Energy Rev.* **2018**, *1*, 461–482. [[CrossRef](#)]

8. Zheng, R.; Wang, W.; Dai, Y.; Ma, Q.; Liu, Y.; Mu, D.; Li, R.; Ren, J.; Dai, C. A closed-loop process for recycling  $\text{LiNi}_x\text{Co}_y\text{Mn}_{(1-x-y)}\text{O}_2$  from mixed cathode materials of lithium-ion batteries. *Green Energy Environ.* **2017**, *2*, 42–50. [[CrossRef](#)]
9. Pagliaro, M.; Meneguzzo, F. Lithium battery reusing and recycling: A circular economy insight. *Heliyon* **2019**, *5*, e01866. [[CrossRef](#)]
10. Ji, Y.; Jafvert, C.T.; Zhao, F. Recovery of cathode materials from spent lithium-ion batteries using eutectic system of lithium compounds. *Resour. Conserv. Recycl.* **2021**, *170*, 105551. [[CrossRef](#)]
11. Bai, Y.; Muralidharan, N.; Sun, Y.-K.; Passerini, S.; Whittingham, M.S.; Belharouak, I. Energy and environmental aspects in recycling lithium-ion batteries: Concept of Battery Identity Global Passport. *Mater. Today* **2020**, *41*, 304–315. [[CrossRef](#)]
12. Zhan, R.; Yang, Z.; Bloom, I.; Pan, L. Significance of a solid electrolyte interphase on separation of anode and cathode materials from spent Li-ion batteries by froth flotation. *ACS Sustain. Chem. Eng.* **2021**, *9*, 531–540. [[CrossRef](#)]
13. Xu, P.; Dai, Q.; Gao, H.; Liu, H.; Zhang, M.; Li, M.; Chen, Y.; An, K.; Meng, Y.S.; Liu, P.; et al. Efficient direct recycling of lithium-ion battery cathodes by targeted healing. *Joule* **2020**, *4*, 2609–2626. [[CrossRef](#)]
14. Nitta, N.; Wu, F.; Lee, J.T.; Yushin, G. Li-ion battery materials: Present and future. *Mater. Today* **2015**, *18*, 252–264. [[CrossRef](#)]
15. Li, J.; Fleetwood, J.; Hawley, W.B.; Kays, W. From materials to cell: State-of-the-art and prospective technologies for lithium-ion battery electrode processing. *Chem. Rev.* **2022**, *122*, 903–956. [[CrossRef](#)]
16. Hawley, W.B.; Li, J. Electrode manufacturing for lithium-ion batteries—Analysis of current and next generation processing. *J. Energy Storage* **2019**, *25*, 100862. [[CrossRef](#)]
17. Blomgren, G.E. The development and future of lithium ion batteries. *J. Electrochem. Soc.* **2017**, *164*, A5019–A5025. [[CrossRef](#)]
18. Shahan, Z. LG Chem Has Begun Mass Production of NCM712. 2020. Available online: <https://cleantechnica.com/2020/06/11/lg-chem-began-mass-production-of-ncm712-batteries-in-poland-in-q1/> (accessed on 11 January 2022).
19. Armand, M.; Axmann, P.; Bresser, D.; Copley, M.; Edstrom, K.; Ekberg, C.; Guyomard, D.; Lestriez, B.; Novak, P.; Petranikova, M.; et al. Lithium-ion batteries—Current state of the art and anticipated developments. *J. Power Sources* **2020**, *479*, 228708. [[CrossRef](#)]
20. Lin, J.; Fan, E.; Zhang, X.; Li, Z.; Dai, Y.; Chen, R.; Wu, F.; Li, L. Sustainable upcycling of spent lithium-ion batteries cathode materials: Stabilization by in situ Li/Mn disorder. *Adv. Energy Mater.* **2022**, *12*, 2201174. [[CrossRef](#)]
21. Wang, T.; Luo, H.; Fan, J.; Thapaliya, B.P.; Bai, Y.; Belharouak, I.; Dai, S. Flux upcycling of spent NMC111 to nickel-rich NMC cathodes in reciprocal ternary molten salts. *iScience* **2022**, *25*, 103801. [[CrossRef](#)]
22. Smith, E.L.; Abbott, A.P.; Ryder, K.S. Deep eutectic solvents (DESs) and their applications. *Chem. Rev.* **2014**, *114*, 11060–11082. [[CrossRef](#)]
23. Fang, X.; Lu, Y.; Ding, N.; Feng, X.Y.; Liu, C.; Chen, C.H. Electrochemical properties of nano- and micro-sized  $\text{LiNi}_{0.5}\text{Mn}_{1.5}\text{O}_4$  synthesized via thermal decomposition of a ternary eutectic Li-Ni-Mn acetate. *Electrochim. Acta* **2010**, *55*, 832–837. [[CrossRef](#)]
24. Li, M.; Wood, D.L.; Bai, Y.; Essehli, R.; Amin, R.; Jafta, C.; Muralidharan, N.; Li, J.; Belharouak, I. Eutectic synthesis of the P2-type  $\text{Na}_x\text{Fe}_{1/2}\text{Mn}_{1/2}\text{O}_2$  cathode with improved cell design for sodium-ion batteries. *ACS Appl. Mater. Interfaces* **2020**, *12*, 23951–23958. [[CrossRef](#)] [[PubMed](#)]
25. Wei, Y.; Zheng, J.; Cui, S.; Song, X.; Su, Y.; Deng, W.; Wu, Z.; Wang, X.; Wang, W.; Rao, M.; et al. Kinetics tuning of Li-ion diffusion in layered  $\text{Li}(\text{Ni}_x\text{Mn}_y\text{Co}_z)\text{O}_2$ . *J. Am. Chem. Soc.* **2015**, *137*, 8364–8367. [[CrossRef](#)] [[PubMed](#)]
26. Liu, Y.; Liu, W.; Zhu, M.; Li, Y.; Li, W.; Zheng, F.; Shen, L.; Dang, M.; Zhang, J. Coating ultra-thin TiN layer onto  $\text{LiNi}_{0.8}\text{Co}_{0.1}\text{Mn}_{0.1}\text{O}_2$  cathode material by atomic layer deposition for high-performance lithium-ion batteries. *J. Alloys Compd.* **2021**, *888*, 161594. [[CrossRef](#)]
27. Shannon, R.D. Revised effective ionic radii and systematic studies of interatomic distances in halides and chalcogenides. *Acta Crystallogr. A* **1976**, *32*, 751–767. [[CrossRef](#)]
28. Qin, X.; Gong, J.; Guo, J.; Zong, B.; Zhou, M.; Wang, L.; Liang, G. Synthesis and performance of  $\text{LiNi}_{0.5}\text{Mn}_{1.5}\text{O}_4$  cathode materials with different particle morphologies and sizes for lithium-ion battery. *J. Alloys Compd.* **2019**, *786*, 240–249. [[CrossRef](#)]
29. Nguyen, T.T.; Kim, U.-H.; Yoon, C.S.; Sun, Y.-K. Enhanced cycling stability of Sn-doped  $\text{Li}[\text{Ni}_{0.90}\text{Co}_{0.05}\text{Mn}_{0.05}]\text{O}_2$  via optimization of particle shape and orientation. *Chem. Eng. J.* **2021**, *405*, 126887. [[CrossRef](#)]
30. Muller, M.; Schneider, L.; Bohn, N.; Binder, J.R.; Bauer, W. Effect of nanostructured and open-porous particle morphology on electrode processing and electrochemical performance of Li-ion batteries. *ACS Appl. Energy Mater.* **2021**, *4*, 1993–2003. [[CrossRef](#)]
31. Li, W.; Liu, X.; Celio, H.; Smith, P.; Dolocan, A.; Chi, M.; Manthiram, A. Mn versus Al in layered oxide cathodes in lithium-ion batteries: A comprehensive evaluation on long-term cyclability. *Adv. Energy Mater.* **2018**, *8*, 1703154. [[CrossRef](#)]
32. Ue, M.; Sakaushi, K.; Uosaki, K. Basic knowledge in battery research bridging the gap between academia and industry. *Mater. Horiz.* **2020**, *7*, 1937–1954. [[CrossRef](#)]
33. Wang, Y.; Roller, J.; Maric, R. Morphology-controlled one-step synthesis of nanostructrued  $\text{LiNi}_{1/3}\text{Mn}_{1/3}\text{Co}_{1/3}\text{O}_2$  electrodes for Li-ion batteries. *ACS Omega* **2018**, *3*, 3966–3973. [[CrossRef](#)] [[PubMed](#)]
34. Hietaniemi, M.; Hu, T.; Valikangas, J.; Niittykoski, J.; Lassi, U. Effect of precursor particle size and morphology on lithiation of  $\text{Ni}_{0.6}\text{Mn}_{0.2}\text{Co}_{0.2}(\text{OH})_2$ . *J. Appl. Electrochem.* **2021**, *51*, 1545–1557. [[CrossRef](#)]

**Disclaimer/Publisher's Note:** The statements, opinions and data contained in all publications are solely those of the individual author(s) and contributor(s) and not of MDPI and/or the editor(s). MDPI and/or the editor(s) disclaim responsibility for any injury to people or property resulting from any ideas, methods, instructions or products referred to in the content.